BOLETIN DE LA SOCIEDAD ESPAÑOLA DE
Cerámica y Vidrio
www.elsevier.es/bsecv

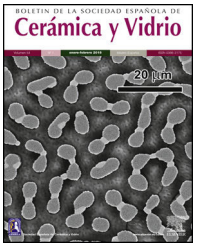

High thermoelectric performances of Bi–AE–Co–O compounds directionally growth from the melt

Juan-Carlos Diez, Shahed Rasekh, Maria A. Madre, Miguel A. Torres, Andres E. Sotelo*

ICMA (CSIC-Universidad de Zaragoza), C/ María de Luna 3, 50018 Zaragoza, Spain

ARTICLE INFO

Article history:
Received 13 July 2017
Accepted 3 October 2017
Available online 27 October 2017

Keywords:
Thermoelectric
Oxide
Directional growth
Electrical properties

ABSTRACT

$Bi_2AE_2Co_2O_x$ (AE = Ca, Sr, and Ba) thermoelectric compounds were grown from the melt by the laser floating zone technique. Microstructural analysis of as-grown samples has shown the formation of well-aligned thermoelectric grains together with a relative high amount of secondary phases. On the other hand, a short (24 h) thermal treatment (810 °C for Sr, 800 °C for Ca, and 750 °C for Ba) under air, raises of thermoelectric phase content through the recombination of the secondary ones. These microstructural modifications led to a large decrease of electrical resistivity, improving the power factor. These results have been compared with samples prepared by the conventional solid state method and with the best values reported in the literature. From these data, it is possible to deduce that the high thermoelectric characteristics obtained in these samples make them very attractive for practical applications.

Altas prestaciones termoeléctricas en compuestos Bi-AE-Co-O crecidos direccionalmente desde el fundido

Palabras clave:
Termoeléctrico
Óxido
Crecimiento direccional
Propiedades eléctricas

RESUMEN

Se han crecido materiales termoeléctricos de la familia Bi2AE2Co2Ox (AE = Ca, Sr y Ba) mediante la técnica de fusión zonal flotante inducida por láser. Los estudios microestructurales han revelado que las muestras crecidas están formadas por granos termoeléctricos bien alineados, acompañados de cantidades apreciables de fases secundarias. Por otro lado, la cantidad de fase termoeléctrica se ha aumentado mediante cortos (24 h) tratamientos térmicos (810 °C para el Sr, 800 °C para el Ca y 750 °C para el Ba) en aire, por reacción de las fases secundarias. Estas modificaciones microestructurales han originado una reducción de la resistividad eléctrica, mejorando el factor de potencia. Los resultados obtenidos se han comparado con los correspondientes a muestras preparadas mediante un proceso clásico en el estado sólido, así como con los mejores resultados que se pueden encontrar en la bibliografía. Todo ello indica que las muestras obtenidas en este trabajo pueden ser muy atractivas para aplicaciones prácticas.

* *Corresponding author.*
E-mail address: monux@unizar.es (J.-C. Diez).
https://doi.org/10.1016/j.bsecv.2017.10.003

Introduction

One of the main characteristics defining the modern civilization is the use and control of large amounts of energy. The current level of development and well-being would be impossible without using abundant and relatively inexpensive energy sources. However, about 2/3 parts of the energy used in conventional conversion/production processes is wasted, mainly as heat. Moreover, more than 80% of the employed energy is based in non-renewable fossil fuels [1]. In this scenario, thermoelectric materials (TE), which are able to directly convert a thermal gradient into electrical energy, could be used to increase the efficiency of such processes and consequently, helping to fight against climate change through a reduction in the of greenhouse gases emission [2]. On the other hand, these TE materials can also be used to produce electrical energy from heat obtained from renewable energy sources as, for example, the sun.

The efficiency of a thermoelectric material is usually described by the so-called dimensionless figure of merit, ZT, defined as $ZT = S^2T/\rho\kappa$, where S is the Seebeck coefficient, T absolute temperature, ρ electrical resistivity, and κ thermal conductivity (electronic and lattice contribution) [3]. In this expression, the electrical part, S^2/ρ, is called power factor, PF, and it is related with the maximum electrical output power which can be obtained from these materials [4].

Since 1997, with the discovery of large TE properties in $NaCo_2O_4$ [5] compound, a great effort of research has been devoted to TE oxides materials, which are very stable in air at high temperatures, as compared to conventional intermetallic ones [6]. Furthermore, these compounds are formed by relatively cheap and environmentally friendly materials [7]. Consequently, many studies on CoO-based materials, with attractive TE properties, such as Ca–Co–O or Bi–AE–Co–O (AE = Ca, Sr, and Ba) have been performed in the last years [8–15]. Their crystal structure can be described as an alternate stacking of two different layers, a common conductive CdI_2-type CoO_2 layer with a two-dimensional triangular lattice, and a block one, composed of insulating rock-salt-type (RS) ones. Both sublattices (RS block and CdI_2-type CoO_2 layer) possess common a- and c-axis lattice parameters and β angles but different b-axis length, causing a misfit along the b-direction [16].

As layered cobaltites are materials with a strong crystallographic anisotropy, the alignment of plate-like grains is necessary to attain properties comparable to those obtained on single crystals. Some techniques have been shown to be useful to obtain a good grain orientation in several TE oxide ceramic systems, such as template grain growth (TTG) [17], hot-pressing [18], spark plasma sintering [19], or directional growth from the melt with an applied electrical current [20]. On the other hand, for these TE oxide ceramics cationic substitution (misfit parameter change) and metallic Ag additions [21–23] have also been found to be favourable for the improvement of their TE properties.

Among all these modern techniques used to obtain highly oriented grains, the laser floating zone (LFZ) technique is well-known as a powerful and reliable one to produce textured materials by directional solidification from the melt. The technique uses a powerful CO_2 or Nd:YAG laser beam as a heat source, producing high-performance materials with well-textured grains from the controlled solidification of a liquid phase (melt) [24]. The main advantages of this technique are the relatively high pulling rates (when compared with conventional techniques, as the Czochralski one) [25], and the possibility of growing advanced, and sometimes complex, ceramic materials with high melting points, such as ZrO_2/Al_2O_3-based eutectics [26], superconductors, e.g. $Bi_2Sr_2CaCu_2O_8$ [27], or more recently on thermoelectric materials, e.g. $Ca_3Co_4O_9$ [28].

In this work we will show the last advances obtained in the Bi–AE–Co–O (AE = Ca, Sr, and Ba) compounds, from a TE point of view, when they are directionally grown from the melt by the laser floating zone technique (LFZ). In order to evaluate the improvements promoted by this technique, a comparison with sintered samples, obtained through the classical solid-state method, will be performed.

Experimental

Classical solid state method

$Bi_2AE_2Co_yO_x$ (AE = Ca, Sr, and Ba) ceramics were prepared by the conventional solid state method using commercial Bi_2O_3 (Panreac, 98+%), CoO (Panreac, 98%) and $CaCO_3$ (Panreac, 98+%), $SrCO_3$ (Panreac, 98+%), or $BaCO_3$ (Panreac, 98+%). They were weighed in the adequate proportions, $y = 1.7$, 1.8 or 2.0 for Ca, Sr, and Ba respectively, in agreement with previously reported data [12]. They were mixed and ball milled at 300 rpm for 30 min in water media. The obtained slurry was placed into a glass container and dried using infrared radiation. The dried mixture was manually milled, and subjected to a two-step thermal treatment (750 and 800 °C for Ca, and Sr, and 700 and 750 °C for Ba) for 12 h, with an intermediate manual milling. This process has been determined in previous studies to be adequate to decompose the alkaline earth carbonates [29]. After thermal treatment, the mixtures were uniaxially pressed at ~400 MPa for 1 min in order to obtain green ceramic parallelepipeds (~3 mm × 3 mm × 14 mm) which are adequate for their thermoelectric characterization. These green bodies were then sintered in the optimal conditions previously determined for these samples [30], and consisting in one step heating at high temperature (810 °C for Sr, 800 °C for Ca, and 750 °C for Ba) for 24 h, under air, with a final furnace cooling.

Texturing through the LFZ process

The polycrystalline ceramics used for this process have been prepared by a sol–gel method route, in order to have very homogeneous initial powders. $Bi(NO_3)_3{\cdot}5H_2O$ (≥98%, Aldrich), $AECO_3$ (AE = Ca, Sr and Ba; 98%, Panreac), and $Co(NO_3)_2{\cdot}6H_2O$ (98%, Panreac) commercial powders were suspended in distilled water. Concentrated HNO_3 (analysis grade, Panreac) was added dropwise into the suspension until it turned into a clear pink solution. Citric acid (99.5%, Panreac), and ethylene glycol (99%, Panreac), were added to this solution in the adequate proportions. Evaporation of the solvent was slowly performed

(between 50 and 100 °C) in order to decompose the nitric acid excess, which allows the polymerization reaction between ethylene glycol and citric acid, forming a pink gel. The dried product was then decomposed (slow self-combustion) by heating at 350 °C for 1 h. The decomposed solid was mechanically ground for 30 min and calcined using the same conditions previously described for the solid-state procedure to decompose the carbonates. This thermal treatment is of critical importance in the LFZ technique in order to avoid the presence of carbonates in the precursors [29]. Otherwise, they would decompose in the molten zone, producing CO_2 bubbles and leading to the crystallization front destabilization. Finally, the powders were cold isostatically pressed into latex tubes at, approximately, 200 MPa for about 2 min to obtain green ceramic cylinders (ϕ ~3 mm and ~100 mm length). These cylinders were subsequently used as feed in an LFZ device equipped with a continuous power Nd:YAG laser (λ = 1064 nm) and optical focussing system (see Fig. 1) described elsewhere in more detail [30]. All LFZ textured samples were processed under the same conditions: 30 mm/h downwards with a seed rotation of 3 rpm to help maintaining the cylindrical geometry. Moreover, in order to assure a good compositional homogeneity of the molten zone, an opposite rotation of 15 rpm was also performed on the feed. After the directional growth process, long (more than 12 cm) and geometrically homogeneous (~2 mm diameter) cylindrical rods were obtained (see Fig. 1). Finally, they were cut into suitably sized pieces for the thermoelectric characterization (~15 mm long).

Annealing of textured samples

As it was determined in previous works in these compounds, the LFZ as-grown materials possess a relatively high amount of secondary phases [29,31,32] as a result of their incongruent melts. As a consequence, some samples were annealed to increase the amount of the thermoelectric phase. In order to compare the results obtained by the different processed samples, the thermal treatment used for each compound has been the same previously described for classically solid-state sintered specimens.

Structural and thermoelectric characterization

The identification of the main phases in all the samples was carried out using powder X-ray diffraction (XRD) analysis in a Rigaku D/max-B X-ray diffractometer (Cu K_α radiation), between 10° and 70°. Microstructural studies have been performed using a field emission scanning electron microscope (FESEM, Zeiss Merlin) equipped with an energy dispersive X-ray spectroscopy (EDS) device, used to qualitatively determine the elemental composition of the different phases. Longitudinal fractured and polished sections of all samples have been observed to analyze their main microstructural.

Electrical resistivity and Seebeck coefficient were simultaneously determined by the standard dc four-probe technique in a LSR-3 measurement system (Linseis GmbH), in the steady state mode, at temperatures ranging from 50 to 650 °C. With the electrical resistivity and Seebeck coefficient data, power factor has been calculated in order to determine the samples performances.

Results and discussion

Powder XRD patterns performed on the three different $Bi_2Ca_2Co_{1.7}O_x$ samples, are presented (from 10 to 40° for clarity) in Fig. 2. From these plots, it is clear that the different procedures used to obtain the samples have minor influence in the results. In all cases the most intense peaks correspond to the *(00l)* planes of the thermoelectric phase, indexed as a monoclinic structure (*P2/m* space group), in agreement with previously reported data [33]. In addition, some minor peaks (marked with a ♦ in Fig. 2) appear mainly in solid-state sintered and LFZ as-grown samples (Fig. 2a and b, respectively).

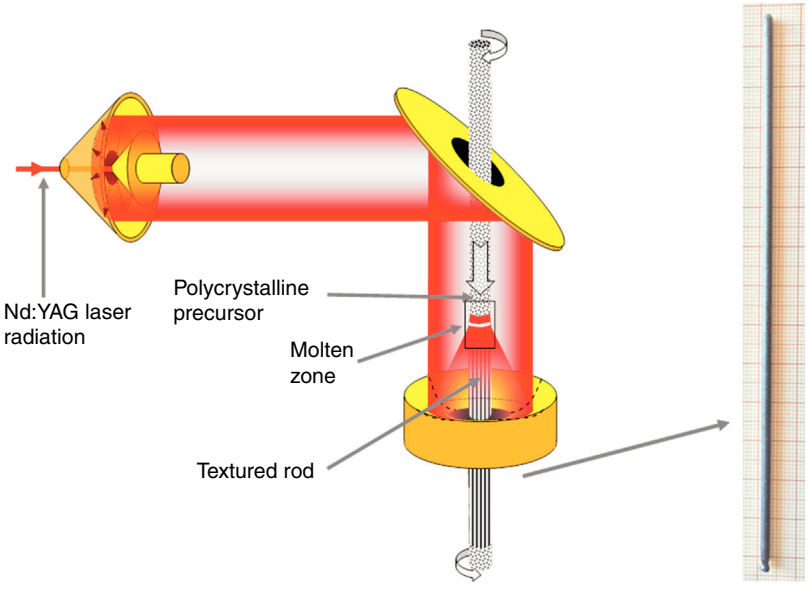

Fig. 1 – Schema of the laser floating zone system used in this work. A typical as-grown Bi–AE–Co–O sample is shown in the right side of the figure.

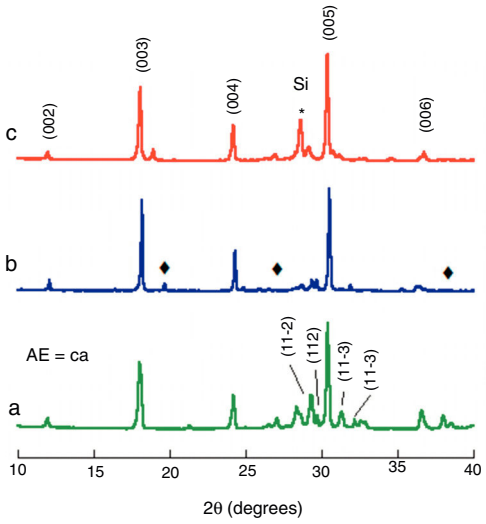

Fig. 2 – Powder XRD patterns of the different $Bi_2Ca_2Co_{1.7}O_x$ samples: (a) solid state sintered, (b) LFZ as-grown, and (c) LFZ annealed. Crystallographic planes indicate the peaks for the $Bi_2Ca_2Co_{1.7}O_x$ TE phase (indexed as *P2/m* space group), ♦ indicates Co-free secondary phase indexed as $Bi_6Ca_4O_{13}$ (*Cmm2* space group), and * indicates the (111) Si peak, added as internal reference.

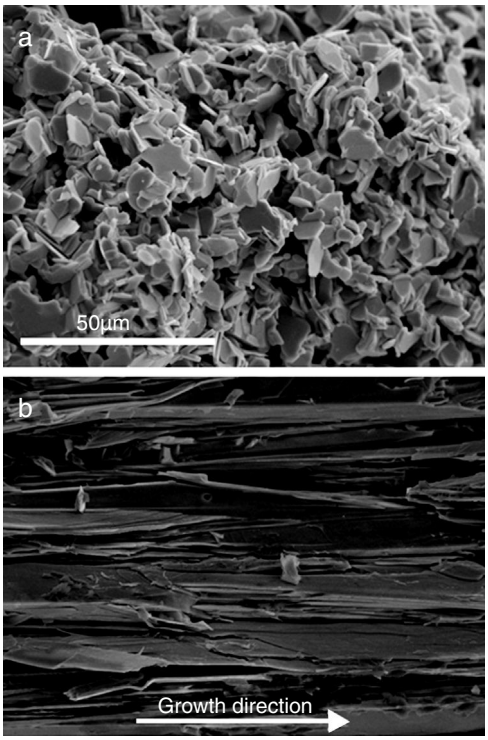

Fig. 3 – Typical FESEM (secondary electrons) micrographs of Bi–AE–Co–O (AE = Ca) fractured surfaces: (a) solid state sintered, and (b) LFZ as-grown (the growth direction is specified by an arrow).

These peaks have been associated to small amounts of Co-free secondary phases ($Bi_6Ca_4O_{13}$ with *Cmm2* space group) [34]. Moreover, no other phases have been identified in any of the samples, indicating that their amount should be very small or, in other case, their peaks should be overlapped with those of the thermoelectric phase. On the other hand, the peak indicated by * corresponds to the *(111)* peak of Si used as internal reference.

The general features described above can be found in all samples, independently of the alkaline-earth cation, with only minor differences. The most intense peaks correspond to the thermoelectric phase, with differences in their relative position due to the different cation sizes. Moreover, the Co-free secondary phases have been identified as Bi_3SrO_y (*R-3mH'*space group) [35], and Bi–Ba–O solid solution (*P121/n1* space group) [36], in their respective samples.

Representative FESEM micrographs of fractured surfaces of sintered and longitudinal as-grown LFZ textured samples are shown in Fig. 3. In these micrographs, the strong differences induced by the two processing methods can be observed. Classically sintered samples (Fig. 3a) show small (5–10 μm in the ab plane) randomly oriented plate-like grains. On the other hand, LFZ as-grown ones possess very large (typically between 50 and 100 μm in the ab plane, depending of the AE cation) and well aligned grains (misalignment below 10°). It should be highlighted that these small misalignments are consequence of the radial thermal gradient appearing at the solidification front due to the relatively large rod diameter [37]. This misalignment could be minimized decreasing the samples diameter or modifying the laser wavelength [38].

Other interesting feature observed at higher magnification, is that these thermoelectric grains are, in turn, composed of very thin plate-like grains perfectly stacked along their *ab* planes. Due to the difficulty to determine the thickness of each individual crystallite by SEM observations, it has been estimated from the XRD results applying Scherrer's formula [39] using the *(005)* peaks of the thermoelectric phase. The calculated mean values are around 50 nm, independently of the alkaline-earth cation and preparation method. These results also confirm that the crystal preferential growth is produced along the *ab* plane.

Representative FESEM micrographs (AE = Ca) of longitudinal polished sections of sintered, as-grown and annealed laser-textured samples are shown in Fig. 4. In these images it is clear that the grain sizes in sintered samples (Fig. 4a) are much lower than for the obtained in laser-textured ones (Fig. 4b and c), confirming the observations described in Fig. 3. Moreover, it can be observed that grey contrast (#1), associated by EDS to the $Bi_2Ca_2Co_{1.7}O_x$ thermoelectric phase, is the major one in the sintered and annealed laser-textured samples (see Fig. 4a and c), while the as-grown ones it is in lower proportion. Light grey contrast (#2) corresponds to $Bi_6Ca_4O_{13}$, present in all samples in different proportions. These observations clearly confirm the previous XRD discussion. On the other hand, black contrast (#3) has been identified as CoO (dendritic grains in Fig. 4b). This phase has not been detected by XRD analyses, probably due to its small proportion. Another important characteristic observed in these micrographs is the different porosity between the samples, it is high in the sintered specimens, while is very low in the laser-textured ones.

These characteristics are maintained in all samples, with only minor differences associated to the alkaline-earth cation.

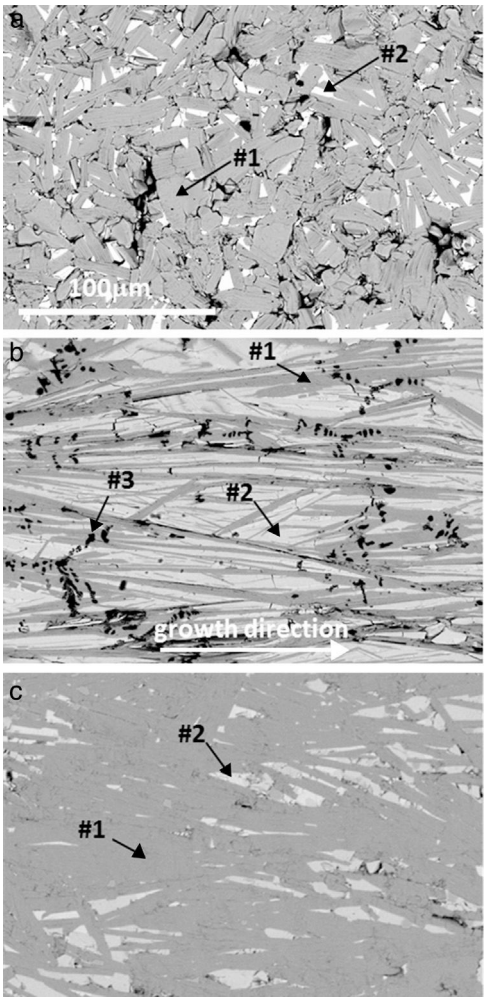

Fig. 4 – Typical FESEM (backscattered electrons) micrographs of Bi–AE–Co–O (AE = Ca) longitudinal polished sections: (a) solid state sintered, (b) LFZ as-grown (the growth direction is specified by an arrow), and (c) annealed laser-textured. Different contrasts are #1: grey one, associated to the thermoelectric $Bi_2Ca_2Co_{1.7}O_x$ phase; #2: light grey, $Bi_6Ca_4O_{13}$; and #3: black, Co-oxide.

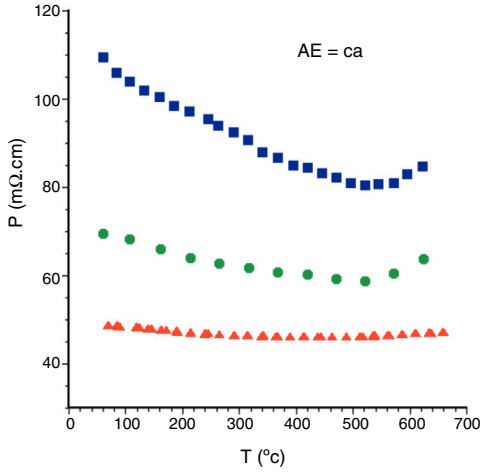

Fig. 5 – Temperature dependence of the electrical resistivity of $Bi_2Ca_2Co_{1.7}O_x$ samples, as a function the processing method: ● solid state sintered, ■ LFZ as-grown and, ▲ LFZ annealed.

Besides the respective thermoelectric phase, the Co-free secondary phase have been identified as Bi_3SrO_y (AE = Sr) [40], and Bi–Ba–O solid solution [41].

These structural and microstructural features are reflected in the electrical properties. The electrical resistivity variation with temperature has been determined and displayed in Fig. 5 for the different $Bi_2Ca_2Co_{1.7}O_x$ samples. As it can be easily observed in the graph, sintered and as-grown samples show similar behaviour in the whole measured temperature range. They behave as semiconductors ($d\rho/dt < 0$) from room temperature to about 500 °C, where the minimum resistivity values are reached, increasing for higher temperatures. In this particular case, the LFZ as-grown samples show higher resistivity values than the sintered ones due to the higher amount of secondary phases. On the other hand, annealed ones display a slight metallic behaviour ($d\rho/dt > 0$) in the whole measured temperature range, and the lowest values (around 46 mΩ cm) among all the Ca samples. This is in agreement with the microstructural data previously discussed previously discussed, which showed that these samples are composed by well-aligned TE grains, together with very small amounts of porosity and secondary phases.

The same general behaviour is found in samples with the other AE cations, the lowest electrical resistivity values are determined in the LFZ annealed samples. The electrical resistivity values at room temperature and 650 °C for the LFZ annealed samples, as a function of the alkaline earth cation, are displayed in Table 1. At a first sight, it is clear that the lowest values have been determined in AE = Ba samples, in agreement with the higher metallicity of these compounds [12]. All these values are low when compared with previously data for polycrystalline samples in the literature, but still far from the single crystal ones. In all cases, the obtained values are lower than the best reported values in sintered materials [42–44], close to the best measured in textured materials using hot forging [17,40,43,44], but higher than the single crystals [12,45]. All these results clearly indicate the good TE quality of these materials.

In order to describe the general S evolution with temperature, in Fig. 6 all Sr samples are presented. In the graph, it is evident that the sign of the Seebeck coefficient is positive for all the samples in the whole measured temperature range, which confirms a conduction mechanism mainly governed by holes. Moreover, the highest room temperature values are obtained for the as-grown samples, due to the higher number of oxygen vacancies in these samples, in agreement with previously reported data [32]. Furthermore, the sintered and the annealed laser-textured samples possess a similar linear behaviour, and values in the whole temperature range, due to their higher content of thermoelectric phase, compared with the as-grown ones. On the other hand, the as-grown samples exhibit a very different behaviour due to the formation of non-equilibrium phases in these samples, as previously observed [40]. These features are maintained independently

Table 1 – Electrical properties of annealed LFZ-textured samples at 50 and 650 °C.

	Electrical resistivity (mΩ cm)		Seebeck coefficient (μV/K)		Power factor × 10^3 (mW/K m)	
	50 °C	650 °C	50 °C	650 °C	50 °C	650 °C
AE = Ca	49	47	169	293	58	182
AE = Sr	18	20	135	202	101	204
AE = Ba	10	9	114	156	130	281

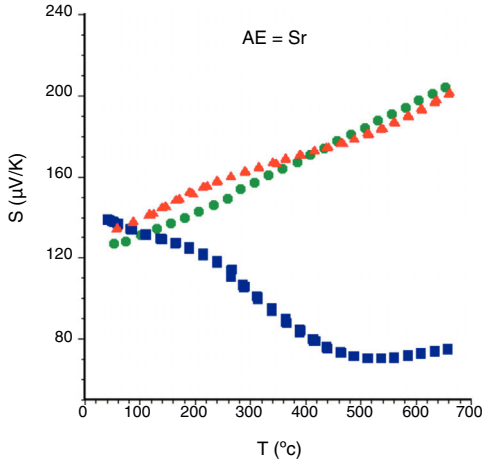

Fig. 6 – Temperature dependence of the Seebeck coefficient of $Bi_2Sr_2Co_{1.8}O_x$ samples, as a function the processing method: ● solid state sintered, ■ LFZ as-grown and, ▲ LFZ annealed.

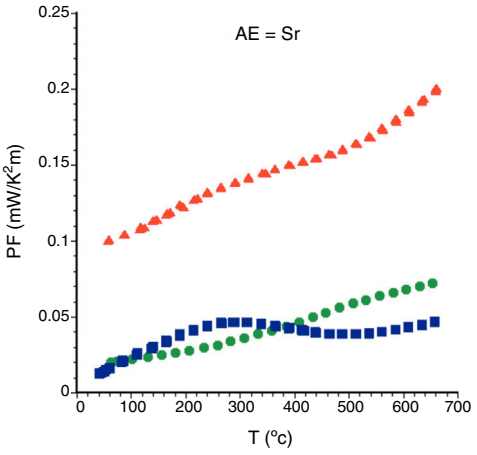

Fig. 7 – Variation of PF with temperature for $Bi_2Sr_2Co_{1.8}O_x$ samples, as a function the processing method: ● solid state sintered, ■ LFZ as-grown and, ▲ LFZ annealed.

of the alkaline earth cation. Moreover, the room temperature values decrease with the increase of AE ionic radii, in agreement with the increase in metallicity [46] and the Koshibae's expression [47]. In Table 1, the S values all for the annealed samples are presented. Even if they are not the highest values obtained in this work for each family, they are higher than the reported in the literature at the same temperatures for single crystals [12,45], hot-forged [17,43,44,48], or sintered materials [42–44].

Finally, from the electrical resistivity and Seebeck coefficient data, PF has been calculated for all samples. Fig. 7 displays the PF evolution, as a function of the temperature, for the Sr samples. As it can be clearly seen, it can be observed that as-grown and sintered samples possess similar values, clearly indicating that the grain alignment is more critical than the content of secondary phases in the thermoelectric performances of these materials. Moreover, when both parameters (grain alignment and phase purity) are improved, the thermoelectric properties are greatly improved, as in the annealed samples. This evolution is maintained, with larger or lower differences in all samples, independently of the alkaline earth cation.

When observing the PF values displayed in Table 1 for the different samples, it is clear that higher metallicity leads to higher performances (Ba samples). In order to know the relative TE performance obtained with these LFZ annealed samples, a comparison with the best data obtained from literature has been performed. In all cases, they are much higher than the obtained in sintered [42–44], and hot-pressed samples [17,44,48], but still lower than the measured in single crystals [12,45].

All these results indicate that some other strategies should be applied, in addition to the LFZ texturing process, in order to obtain closer performances to those obtained in single crystals. Among them, it is possible to highlight Pb doping [49], Ag addition [50] and/or the use of nanosized precursors [51], among others. The success of these combined techniques is evident when considering recent results which combined Pb doping, Ag addition, LFZ texturing, and annealing leading to PF values higher than those obtained in single crystals [52].

Conclusions

It has been demonstrated that $Bi_2AE_2Co_yO_x$ (AE = Ca, Sr, and Ba) ceramics can be adequately textured by the LFZ technique. As these compounds show incongruent melting, in order to produce the TE phase as the major one it is necessary to perform a thermal treatment under air. Moreover, it promotes a great improvement of the thermoelectric properties, compared with the as-grown or the classically sintered materials. From a TE point of view, the properties of these samples are quite attractive for practical applications, with PF values relatively close to those obtained in single crystals.

Acknowledgments

This research has been supported by the Spanish MINECO-FEDER (MAT2013-46505-C3-1-R). The authors wish to thank the Gobierno de Aragón and Fondo Europeo de Desarrollo

Regional (Consolidated Research Groups T87 and T12) for financial support and to C. Gallego, and C. Estepa for their technical assistance. Authors would also like to acknowledge the use of Servicio General de Apoyo a la Investigación-SAI, Universidad de Zaragoza.

REFERENCES

[1] World Energy Outlook 2011, International Energy Agency, Paris, France, 2011.
[2] R. Funahashi, T. Barbier, E. Combe, Thermoelectric materials for middle and high temperature ranges, J. Mater. Res. 30 (2015) 2544–2557, http://dx.doi.org/10.1557/jmr.2015.145.
[3] D.M. Rowe, General principles and basic considerations, in: D.M. Rowe (Ed.), Thermolectrics Handbook: Macro to Nano, CRC Press, Boca Raton, FL, USA, 2006, 1-3–1-7.
[4] D. Nemir, J. Beck, On the significance of the thermoelectric figure of merit Z, J. Electron. Mater. 39 (2010) 1897–1901, http://dx.doi.org/10.1007/s11664-009-1060-4.
[5] I. Terasaki, Y. Sasago, K. Uchinokura, Large thermoelectric power in $NaCo_2O_4$ single crystals, Phys. Rev. B 56 (1997) R12685–R12687, http://dx.doi.org/10.1103/PhysRevB.56.R12685.
[6] K. Kuomoto, R. Funahashi, E. Guilmeau, Y. Miyazaki, A. Weidenkaff, Y.F. Wang, C.L. Wan, Thermoelectric ceramics for energy harvesting, J. Am. Ceram. Soc. 96 (2013) 1–23, http://dx.doi.org/10.1111/jace.12076.
[7] J. He, Y. Liu, R. Funahashi, Oxide thermoelectrics: the challenges, progress, and outlook, J. Mater. Res. 26 (2011) 1762–1772, http://dx.doi.org/10.1557/jmr.2011.108.
[8] Y. Huang, B. Zhao, J. Fang, R. Ang, Y. Sun, Tunning of microstructure and thermoelectric properties of $Ca_3Co_4O_9$ ceramics by high-magnetic-field sintering, J. Appl. Phys. 110 (2011) 123713, http://dx.doi.org/10.1063/1.3671403.
[9] Sh. Rasekh, M.A. Torres, G. Constantinescu, M.A. Madre, J.C. Diez, A. Sotelo, Effect of Cu substitution on $Ca_3Co_4O_9$ thermoelectric ceramics, J. Mater. Sci.-Mater. Electron. 24 (2013) 2309–2314, http://dx.doi.org/10.1007/s10854-013-1094-5.
[10] K. Rubesova, T. Hlasek, V. Jakes, S. Huber, J. Hejtmanek, D. Sedmidubsky, Effect of a powder compaction process on the thermoelectric properties of $Bi_2Sr_2Co_{1.8}O_x$ ceramics, J. Eur. Ceram. Soc. 35 (2015) 525–531, http://dx.doi.org/10.1016/j.jeurceramsoc.2014.08.037.
[11] M.A. Madre, Sh. Rasekh, J.C. Diez, A. Sotelo, New solution method to produce high performance thermoelectric ceramics: a case study of Bi–Sr–Co–O, Mater. Lett. 64 (2010) 2566–2568, http://dx.doi.org/10.1016/j.matlet.2010.08.041.
[12] W. Kobayashi, S. Hebert, H. Muguerra, D. Grebille, D. Pelloquin, A. Maignan, Thermoelectric properties in the misfit-layered-cobalt oxides $[Bi_2A_2O_4]$ $[CoO_2]_{b1/b2}$ (A = Ca, Sr, Ba, b_1/b_2 = 1.65, 1.82, 1.98) single crystals, in: I. Kim (Ed.), Proceedings ICT 07, Twenty-sixth international conference on thermoelectrics, Korea, 2008, pp. 117–120.
[13] A. Sotelo, Sh. Rasekh, M.A. Madre, E. Guilmeau, S. Marinel, J.C. Diez, Solution-based synthesis routes to thermoelectric $Bi_2Ca_2Co_{1.7}O_x$, J. Eur. Ceram. Soc. 31 (2011) 1763–1769, http://dx.doi.org/10.1016/j.jeurceramsoc.2011.03.008.
[14] H. Hao, H. Yang, Y. Liu, X. Hu, High-temperature thermoelectric properties of Cu-substituted $Bi_2Ba_2Co_{2-x}Cu_xO_y$ oxides, J. Mater. Sci. Technol. 27 (2011) 525–528, http://dx.doi.org/10.1016/S1005-0302(11)60102-3.
[15] G. Constantinescu, Sh. Rasekh, M.A. Torres, M.A. Madre, J.C. Diez, A. Sotelo, Enhancement of the high-temperature thermoelectric performance of $Bi_2Ba_2Co_2O_x$, Scr. Mater. 68 (2013) 75–78, http://dx.doi.org/10.1016/j.scriptamat.2012.09.014.
[16] A. Maignan, S. Hebert, M. Hervieu, C. Michel, D. Pelloquin, D. Khomskii, Magnetoresistance and magnetothermopower properties of Bi/Ca/Co/O and Bi(Pb)/Ca/Co/O misfit layer cobaltites, J. Phys.-Condens. Matter 15 (2003) 2711–2723, http://dx.doi.org/10.1088/0953-8984/15/17/323.
[17] H. Itahara, C. Xia, J. Sugiyama, T. Tani, Fabrication of textured thermoelectric layered cobaltites with various rock salt-type layers by using β-$Co(OH)_2$ platelets as reactive templates, J. Mater. Chem. 14 (2004) 61–66, http://dx.doi.org/10.1039/B309804D.
[18] H. Wang, X. Sun, X. Yan, D. Huo, X. Li, J.G. Li, X. Ding, Fabrication and thermoelectric properties of highly textured $Ca_9Co_{12}O_{28}$ ceramic, J. Alloys Compd. 582 (2014) 294–298, http://dx.doi.org/10.1016/j.jallcom.2013.07.145.
[19] N.Y. Wu, T.C. Holgate, N.V. Nong, N. Pryds, S. Linderoth, High temperature thermoelectric properties of $Ca_3Co_4O_{9+\delta}$ by auto-combustion synthesis and spark plasma sintering, J. Eur. Ceram. Soc. 34 (2014) 925–931, http://dx.doi.org/10.1016/j.jeurceramsoc.2013.10.022.
[20] N.M. Ferreira, Sh. Rasekh, F.M. Costa, M.A. Madre, A. Sotelo, J.C. Diez, M.A. Torres, New method to improve the grain alignment and performance of thermoelectric ceramics, Mater. Lett. 83 (2012) 144–147, http://dx.doi.org/10.1016/j.matlet.2012.05.131.
[21] G. Constantinescu, Sh. Rasekh, M.A. Torres, J.C. Diez, M.A. Madre, A. Sotelo, Effect of Sr substitution for Ca on the $Ca_3Co_4O_9$ thermoelectric properties, J. Alloys Compd. 577 (2013) 511–515, http://dx.doi.org/10.1016/j.jallcom.2013.07.005.
[22] A. Sotelo, M.A. Torres, G. Constantinescu, Sh. Rasekh, J.C. Diez, M.A. Madre, Effect of Ag addition on the mechanical and thermoelectric performances of annealed $Bi_2Sr_2Co_{1.8}O_x$ textured ceramics, J. Eur. Ceram. Soc. 32 (2012) 3745–3751, http://dx.doi.org/10.1016/j.jeurceramsoc.2012.05.035.
[23] A. Sotelo, Sh. Rasekh, G. Constantinescu, M.A. Torres, M.A. Madre, J.C. Diez, Improvement of textured $Bi_{1.6}Pb_{0.4}Sr_2Co_{1.8}O_x$ thermoelectric performances by metallic Ag additions, Ceram. Int. 39 (2013) 1597–1602, http://dx.doi.org/10.1016/j.ceramint.2012.07.112.
[24] J.C. Diez, L.A. Angurel, H. Miao, J.M. Fernandez, G.F. de la Fuente, Processing of textured BSCCO superconductors by laser-induced directional solidification, Supercond. Sci. Technol. 11 (1998) 101–106, http://dx.doi.org/10.1088/0953-2048/11/1/020.
[25] R.S. Feigelson, Pulling optical fibers, J. Cryst. Growth 79 (1986) 669–680, http://dx.doi.org/10.1016/0022-0248(86)90535-X.
[26] J.I. Pena, R.I. Merino, N.R. Harlan, A. Larrea, G.F. de la Fuente, V.M. Orera, Microstructure of Y_2O_3 doped Al_2O_3–ZrO_2 eutectics grown by the laser floating zone method, J. Eur. Ceram. Soc. 22 (2002) 2595–2602, http://dx.doi.org/10.1016/S0955-2219(02)00121-8.
[27] M. Mora, E. Martinez, J.C. Diez, L.A. Angurel, G.F. de la Fuente, Phase growth and microstructure modifications induced by annealing in highly textured superconducting Bi-2212 thin rods, J. Mater. Res. 15 (2000) 614–620, http://dx.doi.org/10.1557/JMR. 2000.0091.
[28] M.A. Madre, F.M. Costa, N.M. Ferreira, A. Sotelo, M.A. Torres, G. Constantinescu, Sh. Rasekh, J.C. Diez, Preparation of high-performance $Ca_3Co_4O_9$ thermoelectric ceramics produced by a new two-step method, J. Eur. Ceram. Soc. 33 (2013) 1747–1754, http://dx.doi.org/10.1016/j.jeurceramsoc.2013.01.029.
[29] J.C. Diez, E. Guilmeau, M.A. Madre, S. Marinel, S. Lemonnier, A. Sotelo, Improvement of $Bi_2Sr_2Co_{1.8}O_x$ thermoelectric properties by laser floating zone texturing, Solid State Ion. 180 (2009) 827–830, http://dx.doi.org/10.1016/j.ssi.2009.02.004.

[30] Sh. Rasekh, Tuning up Bi–AE–Co–O (AE: Alkaline Earth) thermoelectric performances via processing and doping (Doctoral Thesis dissertation), University of Zaragoza, Spain, 2016.
[31] A. Sotelo, E. Guilmeau, M.A. Madre, S. Marinel, S. Lemonnier, J.C. Diez, $Bi_2Ca_2Co_{1.7}O_x$ thermoelectric ceramics textured by laser floating zone method, Bol. Soc. Esp. Ceram. Vidr. 47 (2008) 225–228.
[32] Sh. Rasekh, G. Constantinescu, M.A. Torres, M.A. Madre, J.C. Diez, A. Sotelo, Growth rate effect on microstructure and thermoelectric properties of melt grown $Bi_2Ba_2Co_2O_x$ textured ceramics, Adv. Appl. Ceram. 111 (2012) 490–494, http://dx.doi.org/10.1179/1743676112Y.0000000039.
[33] H. Muguerra, D. Grebille, E. Guilmeau, R. Cloots, Modulated misfit structure of the thermoelectric $[Bi_{0.84}CaO_2]2[CoO_2]_{1.69}$ cobalt oxide, Inorg. Chem. 47 (2008) 2464–2471, http://dx.doi.org/10.1021/ic701717f.
[34] J.B. Parise, C.C. Torardi, M.H. Whangbo, C.J. Rawn, R.S. Roth, B.P. Burton, Calcium bismuth oxide ($Ca_4Bi_6O_{13}$), a compound containing an unusually low bismuth coordination number and short Bi–Bi contacts, Chem. Mater. 2 (1990) 454–458, http://dx.doi.org/10.1021/cm00010a026.
[35] D. Mercurio, J.C. Champarnaud-Mesjard, B. Frit, P. Conflant, J.C. Boivin, T. Vogt, Thermal evolution of the crystal structure of the rhombohedral $Bi_{0.75}Sr_{0.25}O_{1.375}$ phase: a single crystal neutron diffraction study, J. Solid State Chem. 112 (1994) 1–8, http://dx.doi.org/10.1006/jssc.1994.1255.
[36] B.J. Kennedy, C.J. Howard, K.S. Knight, Z. Zhang, Q. Zhou, Structures and phase transitions in the ordered double perovskites $Ba_2Bi^{III}Bi^{V}O_6$ and $Ba_2Bi^{III}Sb^{V}O_6$, Acta Crystallogr. Sect. B-Struct. Sci. Cryst. Eng. Mater. 62 (2006) 537–546, http://dx.doi.org/10.1107/S0108768106018842.
[37] F.M. Costa, N.M. Ferreira, Sh. Rasekh, A.J.S. Fernandes, M.A. Torres, M.A. Madre, J.C. Diez, A. Sotelo, Very large superconducting currents induced by growth tailoring, Cryst. Growth Des. 15 (2015) 2094–2101, http://dx.doi.org/10.1021/cg5015972.
[38] G.F. de la Fuente, J.C. Diez, L.A. Angurel, J.I. Peña, A. Sotelo, R. Navarro, Wavelength dependence in laser floating-zone processing. A case study with Bi–Sr–Ca–Cu–O superconductors, Adv. Mater. 7 (1995) 853–856, http://dx.doi.org/10.1002/adma.19950071008.
[39] A.L. Patterson, The Scherrer formula for X-ray particle size determination, Phys. Rev. 56 (1939) 978–982, http://dx.doi.org/10.1103/PhysRev.56.978.
[40] Sh. Rasekh, F.M. Costa, N.M. Ferreira, M.A. Torres, M.A. Madre, J.C. Diez, A. Sotelo, Use of laser technology to produce high thermoelectric performances in $Bi_2Sr_2Co_{1.8}O_x$, Mater. Des. 75 (2015) 143–148, http://dx.doi.org/10.1016/j.matdes.2015.03.005.
[41] J.C. Diez, M.A. Madre, M.A. Torres, Sh. Rasekh, A. Sotelo, Long-term high-temperature stability of directionally grown $[Bi_2Ba_2O_4]_p[CoO_2]$ rods, Materials 10 (2017) 146, http://dx.doi.org/10.3390/ma10020146.
[42] H.S. Hao, H.P. Yu, L.M. Zhao, Thermoelectric characteristics of Pb- and La- doped $Bi_2Ba_2Co_2O_y$ ceramics, Adv. Mater. Res. 228–229 (2011) 804–808, http://dx.doi.org/10.4028/www.scientific.net/AMR.228-229.804.
[43] E. Guilmeau, M. Pollet, D. Grebille, D. Chateigner, B. Vertruyen, R. Cloots, R. Funahashi, B. Ouladiaff, Neutron diffraction texture analysis and thermoelectric properties of BiCaCoO misfit compounds, Mater. Res. Bull. 43 (2008) 394–400, http://dx.doi.org/10.1016/j.materresbull.2007.02.043.
[44] E. Combe, R. Funahashi, F. Azough, R. Freer, Relationship between microstructure and thermoelectric properties of $Bi_2Sr_2Co_2O_x$ bulk materials, J. Mater. Res. 29 (2014) 1376–1382, http://dx.doi.org/10.1557/jmr.2014.135.
[45] N. Sun, S.T. Dong, B.B. Zhang, Y.B. Chen, J. Zhou, S.T. Zhang, Z.B. Gu, S.H. Yao, Y.F. Chen, Intrinsically modified thermoelectric performance of alkaline-earth isovalently substituted $[Bi_2AE_2O_4][CoO_2]_y$ single crystals, J. Appl. Phys. 114 (2013) 043705, http://dx.doi.org/10.1063/1.4816315.
[46] A. Maignan, D. Pelloquin, S. Hebert, Y. Klein, M. Hervieu, Thermoelectric power in misfit cobaltites ceramics: optimization by chemical substitutions, Bol. Soc. Esp. Ceram. Vidr. 45 (2006) 122–125.
[47] W. Koshibae, K. Tsutsui, S. Maekawa, Thermopower in cobalt oxides, Phys. Rev. B 62 (2000) 6869, http://dx.doi.org/10.1103/PhysRevB.62.6869.
[48] T. Motohashi, Y. Nonaka, K. Sakai, M. Karppinen, H. Yamauchi, Fabrication and thermoelectric characteristics of $[(Bi, Pb)_2Ba_2O_{4\pm w}]_{0.5}CoO_2$ bulks with highly aligned grain structure, J. Appl. Phys. 103 (2008) 033705, http://dx.doi.org/10.1063/1.2838161.
[49] A. Sotelo, E. Guilmeau, Sh. Rasekh, M.A. Madre, S. Marinel, J.C. Diez, Enhancement of the thermoelectric properties of directionally grown Bi–Ca–Co–O through Pb for Bi substitution, J. Eur. Ceram. Soc. 30 (2010) 1815–1820, http://dx.doi.org/10.1016/j.jeurceramsoc.2010.01.037.
[50] D. Flahaut, J. Allouche, A. Sotelo, Sh. Rasekh, M.A. Torres, M.A. Madre, J.C. Diez, Role of tAg in textured-annealed $Bi_2Ca_2Co_{1.7}O_x$ thermoelectric ceramics, Acta Mater. 102 (2016) 273–283, http://dx.doi.org/10.1016/j.actamat.2015.09.036.
[51] A. Sotelo, M.A. Torres, Sh. Rasekh, M.A. madre, J.C. Diez, Effect of precursors on the microstructure and electrical properties of $Bi_2Ba_2Co_2O_x$, J. Aust. Ceram. Soc. (2017), http://dx.doi.org/10.1007/s41779-017-0070-6.
[52] M.A. Madre, F.M. Costa, N.M. Ferreira, S.I.R. Costa, Sh. Rasekh, M.A. Torres, J.C. Diez, V.S. Amaral, J.S. Amaral, A. Sotelo, High thermoelectric performance in $Bi_{2-x}Pb_xBa_2Co_2O_y$ promoted by directional growth and annealing, J. Eur. Ceram. Soc. 36 (2016) 67–74, http://dx.doi.org/10.1016/j.jeurceramsoc.2015.09.034.